Bioconjugate Chemistry

Article

Cite This: Bioconjugate Chem. 2019, 30, 853−860

pubs.acs.org/bc

Shape Matters: Gold Nanoparticle Shape Impacts the Biological Activity of siRNA Delivery

Erin Morgan,[†,#] Dominik Wupperfeld,[†,¶,#] Demosthenes Morales,[†,§] and Norbert Reich*[,†]

[†]Department of Chemistry and Biochemistry, University of California Santa Barbara, Santa Barbara, California 93106, United States

[§]Center for Integrated Nanotechnologies, Los Alamos National Laboratory, Los Alamos, New Mexico 87545, United States

Supporting Information

ABSTRACT: Plasmon-resonant nanoparticles provide unprecedented spatiotemporal control over the release of diverse cargoes into cells. Here we compare the loading, release and internalization efficiencies, and effectiveness of post transcriptional gene silencing of hollow gold nanoshells, hollow gold nanocages, and gold nanorods with plasmons tuned to absorb near-infrared light at 800 nm. The hollow gold nanoshells can be loaded with up to three times more siRNA cargo compared to nanocages and nanorods; however, nanorods exhibit the highest efficiency of release of attached siRNA strands when exposed to pulsed 800 nm laser excitation. In cellular treatments, all particles demonstrated efficient internalization into HeLa cells, but the nanoshells and nanocages display the highest downregulation of GFP expression 72 h after treatment. These results provide novel insights into the relative efficiencies of three structurally distinct types of gold nanoparticles as siRNA carriers and we examine different parameters that may influence their efficacy.

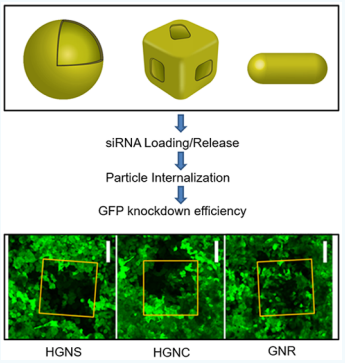

INTRODUCTION

Oligonucleotides, including small interfering RNA (siRNA), micro RNA (miRNA) antisense DNA, and guide RNA (gRNA), are powerful technologies for gene regulation in basic cell research, cancer therapy, and regenerative medicine.[1−4] RNA silencing is a commonly used approach to knock down specific target proteins[5] like cyclin dependent kinases (CDKs), insulin growth factors (IGF, vascular endothelial growth factors (VEGF), and antiapoptotic factors.[6] However, functional siRNA requires an efficient delivery vehicle due to its bioinstability, inefficient accumulation in target tissues, and inability to cross cell membranes to access the cytoplasm.[7−9] Here we compare the relative effectiveness of three types of gold nanoparticles to deliver siRNA based gene knockdown in cancer cells.

Gold nanoparticles have attracted attention in biomedicine and basic science due to their relatively small size, biocompatibility, synthetic versatility, and ease of functionalization for targeting and delivery. Moreover, the ability for light controlled release makes gold nanoparticles a valuable tool for biological applications. By varying the size and the shape of the gold nanoparticles, their surface plasmon resonance (SPR) can be tuned to a desired wavelength. Previously, we demonstrated the attachment and controlled release of thiol labeled cargo from gold surfaces using near-infrared (NIR) light following endocytotic uptake, providing a compelling platform for the delivery of peptides, proteins, and bioactive DNA and RNA.[10−14] The ability to fine-tune optical properties of various gold nanoparticles is well documented,[15−17] resulting in distinctive localized surface plasmons, with wavelengths ranging from the visible to the near-infrared (NIR). The exposure of gold nanoparticles to femtosecond pulsed NIR laser irradiation generates an oscillation of electrons on the surface of the particle which cleaves the gold−thiol bond.[18−20] After cellular internalization of the particles with a cell-penetrating peptide (TAT),[10] NIR light irradiation releases the double-stranded siRNA from the nanoparticle's surface and facilitates endosomal escape to initiate gene silencing activity, with no detectable cell damage.[11,21] The endosomal release arises through membrane disruption caused by a plasmonic heating of a nanometer-sized shell of water surrounding the surface of the particles generating localized nanobubbles. These nanobubbles allow for disruption of the endosomal barrier without causing a bulk heating effect to the cell.[12,13,21]

Prior characterization of gold nanorods and hollow gold nanoshells using continuous irradiation (rather than the pulsed laser used in this study) showed that light-triggered and thermally induced release are observed with nanoshell-based complexes, whereas for nanorod complexes, no analogous release was detectable below the melting temperature of the DNA.[22] Other studies have compared the physical and optical properties of different gold nanoparticles, the effect on photothermal therapy (PTT) and overall internalization.[21] However, the effect of delivery of siRNA for knockdown applications beyond cytotoxicity by various nanoparticles has not been described.[21] Christie et. al compared the effect of nanoparticle shape on PTT of gold nanorods and gold nanoshells and determined that even though gold nanorods were internalized more efficiently into macrophages, the gold nanoshells were more effective at PTT.[23] A recent study

Received: January 3, 2019
Revised: January 30, 2019
Published: February 8, 2019

DOI: 10.1021/acs.bioconjchem.9b00004
Bioconjugate Chem. 2019, 30, 853−860

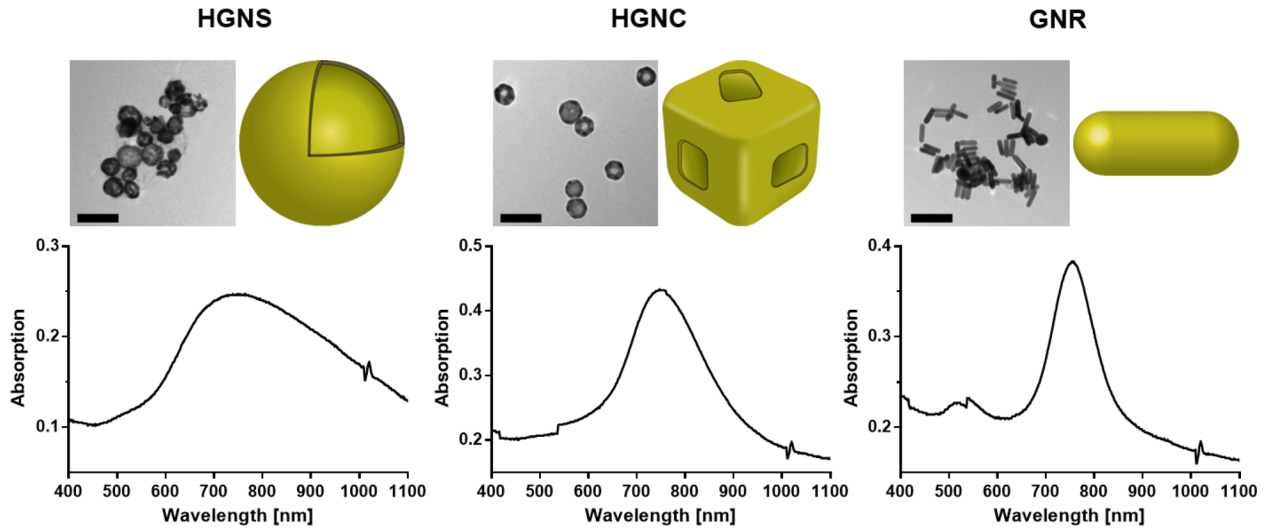

Figure 1. Characterization of hollow gold nanoshells (HGNS), hollow gold nanocages (HGNC), and gold nanorods (GNR). Transmission electron microscope (TEM) imaging of gold nanoparticles depicts characteristic hollow structures of HGNS and HGNC as evidenced by the decreased electron density at the centers of the particles, while GNR are confirmed to be rod-like. TEM images (JEOL 1230 TEM) are accompanied by UV−vis absorption spectra showing primary plasmon peaks at ∼750 nm for each class of nanoparticle. Average size of each gold nanoparticle is ∼45 nm (TEM scale bar is 100 nm, n = 20).

compared the cellular uptake and distribution of gold particles of different sizes and found that larger particles (40−50 nm) have greater potential as delivery vehicles for siRNA compared to smaller (15 nm) particles due to the quantity of particles internalized.[24] Lacking from prior studies is a comparison of particles of the same size yet different shapes in their ability to load and release their cargo, cellular uptake, and their ability to cause the desired biological change (e.g., post-transcriptional knockdown). The importance of shape has been studied for polymer based particles showing that coblock polymer nanoparticles with worm-like micelles allow for higher transfection efficiencies in rat liver.[25] Others have shown that a shape transformation from long worm and rod-like morphologies to more condensed nanoparticles with spherical and short-rod morphologies leads to improved transfection efficiency.[26] These studies lead us to investigate further the impact of shape on delivery efficiency of siRNA with gold nanoparticles.

We sought to determine which of the three ∼45-nm-diameter gold nanoparticles (hollow gold nanoshells (HGNS), hollow gold nanocages (HGNC), and gold nanorods (GNR)) is most suitable for gene regulation in mammalian cells. Selection criteria were based on loading capacity, release efficiency after laser irradiation, and efficiency of internalization into HeLa-GFP cells as well as the subsequent knockdown of the green fluorescent protein (GFP) with siRNA upon treatment. To maintain uniformity using siRNA on different particle shapes, we used the same number of gold particles with the maximum amount of siRNA loaded in each experimental scenario.

RESULTS AND DISCUSSION

Gold Nanoparticle Characterization. HGNS, HGNC, and GNR (45−50 nm diameter) were prepared (Figure 1). UV−vis spectroscopy was used to determine that each type of gold particle contains a characteristic surface plasmon peak at around 800 nm, optimal for NIR excitation and siRNA release. The HGNS exhibit a single yet broad resonance peak at ∼750 nm due to size variations which can be seen in the transmission electron microscopy (TEM) image in Figure 1. The HGNC also have a main resonance peak at 750 nm and display a hexagonal shape shown by the TEM image in Figure 1. The hexagonal shape is due to truncation of the cube's corners and edges during the galvanic replacement reaction.[27] Finally, the GNR have a main longitudinal surface plasmon peak at ∼750 nm as well as a second transversal plasmon peak at ∼520 nm.[28,29]

Load and Release of siRNA. A clear advantage of nanoparticle-based delivery of bioactive nucleic acids is that one particle can be loaded with many copies of the nucleic acid. Using thiol-modified oligonucleotides, two common assembly methods were tested and the oligonucleotide concentrations were increased to maximize the loading of each gold nanoparticle (Figure S1). The loading of the thiolated oligonucleotides relied on a consistent use of 32×10^{-12} M particles, while the loading conditions for each particle were varied to ensure each particle shape had the maximum amount of siRNA on the surface. Each particle type was treated with either a low pH-induced adsorption followed by a buffer exchange where the particles were spun down and resuspended in HEPES buffer (assembly method 1) or a low pH-induced absorption in combination with SDS (sodium dodecyl sulfate) and TBE (Tris, boric acid, and EDTA) (assembly method 2).[16,28] Assembly method 1 appeared to be optimal for decorating siRNA onto HGNS only (Figure S1).[19,30] The GNR on the other hand exhibited instability after treatment, reflected by a blue-shift in the UV−vis spectra, indicative of flocculation of the particles (Figure S1), and therefore was not used for GNR-siRNA assembly. Assembly method 2 delivered the best results for increasing siRNA loading on the GNR and HGNC but not for HGNS. Thus, buffer exchange with HEPES was used for further HGNS preparations, while SDS/TBE was employed for the GNR and HGNC. This would suggest that the initial capping agent used during the synthesis of the gold nanoparticles determines the optimum buffer for the exchange. Assembly method 1 worked best for the HGNS, as they were initially capped with citrate during synthesis. However, the GNR and HGNC require

DOI: 10.1021/acs.bioconjchem.9b00004
Bioconjugate Chem. 2019, 30, 853−860

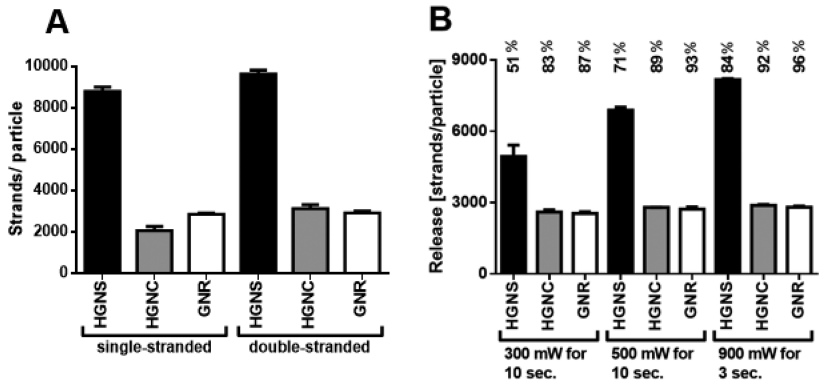

Figure 2. HGNS show the highest level of loading and absolute quantity of siRNA release compared to HGNC and GNR with Qubit assay. (A) Total siRNA loaded onto 3.2 pM particles determined after dissolution with a solution containing KCN, after initial loading of 3 μM siRNA (1000× the max loading capacity of siRNA calculated). (B) Release of loaded siRNA from 3.2 pM gold nanoparticles after exposure to 800 nm femtosecond pulsed NIR laser light. Percent release from each particle is indicated above each bar (n = 6).

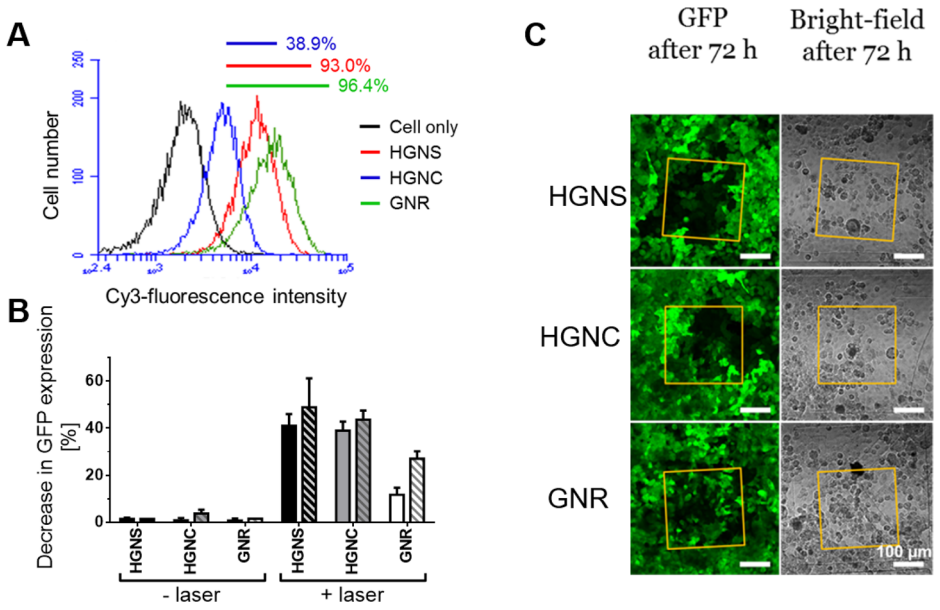

Figure 3. HGNS and HGNC show comparable and superior gene knockdown efficiencies over GNR. (A) Flow cytometry histograms of internalization efficiencies of the different gold nanoparticles into HeLa cells as described by changes in fluorescence profiles due to Cy3 labeled particle uptake. Percentage of cells with Cy3 internalized shown for each type of gold nanoparticle was determined via flow cytometry. (B) Quantitative determination of the decreased GFP expression after knockdown in HeLa-GFP cells via flow cytometry. Percent decrease in GFP expression determined from the number of cells not fluorescent 3 days after treatment of HeLa-GFP cells with a particle concentration of 3.8×10^{-12} M (solid bar) or 7.6×10^{-12} M (striped bar). (C) Spatially controlled knockdown of GFP using NIR excitation by confocal microscopy. GFP-fluorescence (green) and bright-field (gray) microscopy images of HeLa-GFP cells 3 days after siRNA release (yellow square) for GFP-knockdown treated with the different gold nanoparticles. Scale bar in the microscopy images is 100 μm.

capping agents such as CTAB and polyvinylpyrrolidone (PVP), respectively, which allows the use of stringent reagents such as SDS without particle flocculation. Figure 2A shows the maximum ssRNA and dsRNA observed per particle for each of the three particle shapes quantified using a Qubit fluorescence assay (Invitrogen). Single stranded and double stranded RNA are presented in Figure 2 to demonstrate that the dsRNA quantitated in the loading experiment is solely due to the hybridization of the complement to the single strand attached to the particle rather than nonspecific interaction with the particle surface. Loading of HGNS (~8000 strands per particle) with both single and double stranded nucleic acids was significantly greater than for HGNC and GNR (~3000 strands per particle for each). This is likely to impact various features of their delivery into cells (e.g., stability of RNA, particle internalization, and efficiency of knockdown).

The siRNA release efficiency of each gold nanoparticle was determined by measuring the quantity of dsRNA in the supernatant of the sample after laser irradiation per gold nanoparticle (Figure 2B). Against expectations, the high loading of siRNA onto the HGNS seen in Figure 2A had lowest percentage (51%) of total dsRNA released with low laser power compared to HGNC and GNR (83% and 87%, respectively). The low percentage of siRNA released from HGNS was increased dramatically (85%) when the laser power was increased while the other particles did not see as dramatic of an increase with an increase in laser power (Figure 2B). The release percent for higher power laser excitation of HGNS (85%) is typical as seen by Braun et. al and Morales et al.[13,31]

DOI: 10.1021/acs.bioconjchem.9b00004
Bioconjugate Chem. 2019, 30, 853−860

Influence of Particle Shape on TAT-Mediated Endocytosis. Size, shape, and surface properties influence the internalization of particles into cells.[32,31] Previous studies lacked the comparison of the three different shapes of particles used in this study with similar dimensions. The influence of particle shape on internalization was determined quantitatively through flow cytometry (Figure 3A) and qualitatively through fluorescence microscopy (Figure S2). For cellular studies, the adsorbed thiol oligonucleotides on the gold surfaces were hybridized at a 1:1 ratio with complementary sequences, one of which was labeled with a Cy3 dye for tracking, the other was labeled with a biotin tag for further functionalization with streptavidin and biotin-TAT. Note that in this case the Cy3 was added to the nanoparticles via the fluorescently labeled complement strand for the siRNA already attached to the particle whereas the quantification of dsRNA released from the particles was stated in Figure 2b using the qubit assay (no fluorescent label). The qubit method is a standard for quantification of nucleic acid in a sample and was thus used to quantitate the amount of siRNA bound to each particle shape. Previous work conducted by Huang et al. demonstrates the same amount of Cy3-siRNA is quantified using a fluorescence based assay on HGNs.[10] Since these values are consistent for the HGNs across the two different quantification methods and the same complement sequence was used in this study.

The TAT peptide is well characterized to promote cellular uptake and our previous studies determined that a 1:1 ratio was optimal for internalization and sufficient for siRNA knockdown.[13] HeLa cells were treated with HGNS, GNR, and HGNC for 2 h and then characterized by flow cytometry to measure the degree of gold nanoparticle uptake determined by the increase in cell population exhibiting Cy3 fluorescence (Figure 3A). High incidence of Cy3 fluorescence was observed in 96% of cells that were treated with GNR, while 93% of cells exhibited Cy3 when treated with HGNS. On the other hand, only 39% of HGNC treated cells showed noticeable changes in fluorescence intensity.

Internalization was also investigated by darkfield microscopy in which the gold nanoparticles are visible as bright, orange dots inside the HeLa cells due to light scattering (Figure S2). Complementary fluorescence microscopy imaging mirrors the internalization results acquired through flow cytometry in Figure 3A with GNR and HGNS internalized best. However, dark field microscopy showed a discrepancy with the flow cytometry analysis in the amount of GNR internalized relative to the HGNS and reduced numbers of GNR were observed from imaging. The Cy3 fluorescence observed by flow cytometry (Figure 3A) may be affected by the ability of gold nanoparticles to either quench or enhance fluorescent dyes close to particle surfaces.[26] GNR have been observed to enhance the fluorescence dyes on their surface and therefore lead to seemingly higher internalization as analyzed by cytometry.[33] The enhancement of the Cy3 dye on the surface of GNR as well as the dark-field microscopy data agree with the literature and indicate that less GNR are internalized into HeLa cells than HGNC and HGNS.

Efficiency of siRNA Delivery for GFP Knockdown in HeLa Cells. A final comparison of the three gold nanoparticles tested the overall efficiency of gene knockdown, which includes all of the features tested independently up to this point (loading, release, and internalization). The number of particles used in the treatment was kept constant and two irradiation methods were used. The ensemble laser treatment relied on cells passed through a capillary tube underneath the path of the NIR laser beam (Figure 3B). The second setup used the two-photon microscope equipped with a mode-locked titanium-sapphire femtosecond (fs) tunable (690−1020 nm) pulsed laser to control when and where the gene knockdown occurs for qualitative knockdown studies (Figure 3C). Experiments were conducted using both adherent and suspension cells. The two-photon irradiation method used adherent cells to demonstrate control over the area for knockdown (Figure 3C). The suspension cell system used to determine the percent knockdown efficiency of each particle shape (Figure 3B) allowed for bulk irradiation of the cells passed through a microfluidic device and later quantification of knockdown efficiency using flow cytometry.

GFP-knockdown was observed for the ensemble laser irradiation method with all three gold nanoparticle shapes via flow cytometry. The no laser control, which had particles internalized but which were not irradiated with NIR light, showed no GFP knockdown (Figure 3B). GNR showed the smallest percent decrease in GFP knockdown. Both HGNS and HGNC had comparable knockdown efficiencies and each showed a slight increase in GFP knockdown efficiency with a higher particle concentration indicating the efficiencies were saturated with HGNS and HGNC. GNR showed a doubling in GFP knockdown with a doubling of particle concentration. Thus, more particles are required for GNR-induced GFP knockdown compared to HGNS and HGNC which agrees with the enhanced Cy3 dye effect of GNR observed in Figure S2.

The two-photon microscope results in Figure 3C used an Ibidi gridded cell culture dish that offers the opportunity to irradiate the HeLa-GFP cells in a specific area and relocate them 72 h later. This experiment was used to complement the flow cytometry data and show the GFP knockdown. HeLa-GFP cells with internalized gold nanoparticles showed patterns of GFP knockdown in areas of irradiation after 72 h (Figure 3C). Cell culture areas treated with HGNS or HGNC show clear nonfluorescent spots in the irradiation areas while the GNR samples exhibit only slightly less fluorescence in the area of irradiation with a lot of green fluorescent cells in between. Samples without gold nanoparticles showed no decrease in fluorescence after 72 h (Figure S3). The targeted knockdown using the two-photon microscope again confirms that the GNR do not exhibit the same knockdown capabilities as the HGNS and HGNC.

■ CONCLUSION

We observed the effect of gold nanoparticle shape on siRNA delivery through studying their loading and release efficiencies and internalization efficiencies and determined how these results affect the overall knockdown efficiency of GFP in HeLa cells. After maximizing the amount of siRNA loaded onto each type of gold nanoparticle, HGNS were found to load more than three times the amount of siRNA strands compared to HGNC and GNR. Despite the increase in siRNA loading on the HGN, the overall knockdown efficiency of the HGN compared to the HGNC was similar. In addition, we found that the shape of the particle strongly affected the internalization of the gold nanoparticles of similar size resulting in an observable change in the number of particles internalized to HeLa cells. When the HeLa cells were treated with a consistent number of gold nanoparticles across the different shapes, the

DOI: 10.1021/acs.bioconjchem.9b00004
Bioconjugate Chem. 2019, 30, 853−860

final GFP knockdown results showed that GNR were the least efficient at GFP knockdown. This data in combination with the decrease in internalization seen for the GNR shows the importance of high particle internalization over loading/release for efficient gene knockdown using gold nanoparticles.

EXPERIMENTAL PROCEDURES

Synthesis of the Different Gold Nanoparticles. The HGNS are porous with a hollow core formed by a gold galvanic exchange initiating at the surface of silver precursor nanoparticles and were synthesized as described earlier.[34] Porous and HGNC were made by synthesizing silver nanocubes and subsequent conversion into hollow gold nanocages by galvanic replacement reaction as described earlier.[35] The synthesis and purification of the GNR was carried out with the rapid modification at low pH method, described before.[36] For the experiments all working solutions had to be ribonuclease (RNase)-free. The HGNS as well as HGNC were dialyzed overnight in sodium citrate dialysis buffer (500×10^{-6} M) with 0.03% diethyl dicarbonate (DEPC) with dialysis cassettes (molecular weight cutoff (MWCO) of 20,000). GNR were not synthesized in a RNase-free environment and afterward purified with RNase-free solutions.

Functionalization of the Nanoparticles. *Deprotection of RNA/DNA.* The disulfide protecting group on each oligonucleotide (DNA/RNA) was removed by incubating 12.5×10^{-3} M tris (2-carboxyethyl)phosphine HCl (TCEP) with 100×10^{-6} M DNA/RNA strands at room temperature (RT) for 20 min followed by a chloroform extraction (4×1000 μL). The freshly reduced thiol-modified RNA or DNA was afterward added to the differently shaped particles.

Attachment of RNA/DNA. Assembly method 1: For the attachment onto the surface of HGNS 3×10^{-6} M deprotected RNA or DNA was added to HGNS with an optical density (OD) of 1 (correspond to $\sim 3.58 \times 10^{8}$ HGNS/mL) in the presence of 10×10^{-3} M sodium citrate-HCl (Na_3Cit-HCl), and incubated at RT for 20 min after brief sonication. Afterward, the pH was neutralized by adding 130×10^{-3} M HEPES buffer, the solution was gradually salted to 1 M Na^+ within 20 min using 3.0 M sodium chloride (NaCl), 0.3 M sodium citrate (Na_3Cit) pH 7.0 (20 × SSC), in the presence of 0.01% Tween-20 and 1×10^{-3} M magnesium chloride ($MgCl_2$). Unbound RNA/DNA strands were removed by washing the HGNS twice in washing buffer (1×10^{-3} M $MgCl_2$, 0.01% Tween-20, 300×10^{-3} M NaCl, and 30×10^{-3} M Na_3Cit pH 7). All washing steps were performed by centrifuging at 7000*g* for 10 min followed by brief sonication. After the last centrifugation step, the particles were resuspended in the hybridization buffer (10×10^{-3} M $MgCl_2$ and 600×10^{-3} M Na^+).

For the attachment of RNA/DNA onto the surface of HGNC and GNR first, 1 × TBE buffer, 500 mM NaCl, and 0.02% SDS were mixed together and inverted by hand. Hydrochloric acid (HCl) was used to adjust the mixture's pH to 3.0. To this solution both 3×10^{-6} M of deprotected RNA/DNA as well as 1 OD of HGNC (correspond to $\sim 2.52 \times 10^{8}$ HGNC/mL) or GNR (correspond to $\sim 6.53 \times 10^{8}$ GNR/mL) were added and incubated in the dark for 40 h. Afterward, unbound RNA/DNA strands were removed by washing the HGNC and GNR twice in washing buffer followed by brief sonication. After the last centrifugation step, the particles were resuspended in the hybridization buffer.

Hybridization of Complementary RNA/DNA Strand. Complementary RNA or DNA (1×10^{-6} M) were added to the single-stranded RNA/DNA assembled particle solution (1 OD HGNS, HGNC, or GNR) in hybridization buffer followed by an incubation at 70 °C for 2 min and an immediate incubation at 45 °C for 30 min. Excess complementary RNA/DNA strands were washed out by centrifuging 2× at 7000*g* for 10 min, using 0.1% Tween-20 in Dulbecco's phosphate-buffered saline (PBST).

For the particles with RNA assembled on the surface, an additional step was carried out to functionalize the 3′-end of the thiol-RNA with biotin. The particles were resuspended in conjugation buffer (10×10^{-3} M HEPES pH 7.5, 1×10^{-3} M $MgCl_2$, 0.01% Tween-20) after the last washing step. Afterward, a large excess of 127×10^{-6} M NHS-PEG_4-Biotin (Thermo SCIENTIFIC) in dimethyl sulfoxide (DMSO) was added to the particles with RNA to complete the functionalization of the particle. The solution was sonicated briefly and incubated for 1 h at room temperature followed by washing with conjugation buffer twice to remove excess biotin reagent.

Functionalization with Streptavidin and Biotin-TAT. Streptavidin was added at 2 mg/mL to 32×10^{-12} M gold nanoparticles in the presence of 0.5x PBST, 33.5×10^{-3} M HEPES buffer, and 335×10^{-6} M $MgCl_2$. To avoid self-aggregation of the particles caused by streptavidin bridging, the solution was vortexed and sonicated immediately upon the addition of streptavidin and incubated at RT for 1 h. Afterward, the gold nanoparticles were washed twice with PBST at 4 °C. 15×10^{-6} M of biotin-TAT (N-terminal biotin, YGRKKRRQRRR, GenScript) was added twice to 32 pM of nanoparticles in 0.5× PBST and 50×10^{-3} M HEPES buffer followed by brief sonication and 30 min of incubation at RT. The resulting functionalized gold nanoparticles were washed with PBST and stored at 4 °C prior to cell use.

UV−vis Absorbance Spectra. For the absorbance spectra, the gold nanoparticles were diluted in water and the measurement was carried out with a UV−vis spectrometer (PharmaSpec instrument with a UV-1700, Shimadzu) at a wavelength from 400 to 1100 nm for each different gold nanoparticle type.

TEM. For the detection of the different kinds of gold nanoparticles, 3×10^{-6} L of each particle sample (3.2×10^{-12} M) was pipetted onto a carbon-covered TEM copper mesh grid (SPI Supplies) and stored at RT until the whole solvent (water) was evaporated. Afterward, the grids were brought into the JEOL JEM-1230 TEM (JEOL) to image the different kinds of gold nanoparticles with a voltage of 80 kV and a 150,000 × magnification.

Detection of DNA/RNA Concentration. For the determination of the amount of oligonucleotides attached onto the surface of the different kinds of gold nanoparticles, a KCN etch was performed. The particles were etched by potassium cyanide (KCN) solution (20×10^{-3} M KCN, 200×10^{-6} M $K_3Fe(CN)_6$) to completely release the coated RNA/DNA. Afterward, the RNA/DNA concentration can be determined with the Qubit ssDNA Assay Kit (Invitrogen). For these measurements, the ssDNA Reagent was diluted 1:200 in ssDNA Buffer (working solution). Then, the samples were diluted 1:10 in the working solution and afterward measured at the Qubit 3.0 Fluorometer (Invitrogen).

Bulk Pulsed NIR-Laser Irradiation for Cell Free Release Studies. Release experiments were carried out with

DOI: 10.1021/acs.bioconjchem.9b00004
Bioconjugate Chem. 2019, 30, 853−860

gold nanoparticle solutions in the presence of 0.1×10^{-3}g/10^{-3}L bovine serum albumin (BSA). The samples were irradiated with a pulsed laser generated from a femtosecond Ti:sapphire regenerative amplifier (Spectraphysics Spitfire) running at 1 kHz repetition rate with a Gaussian beam diameter of 5 mm. Pulse duration was kept to 130 fs and the spectral full width at half-maximum of the laser radiation was 12 nm centered around 800 nm. The laser was directed onto the sample by a series of mirrors, and no focusing optics were used. The laser power was measured with a thermopile power meter (Newport Inc.). After laser irradiation, the samples were centrifuged down to separate the released DNA/RNA strands in the supernatant from the gold nanoparticle pellet.

Cell Culture. Both HeLa cells as well as HeLa-GFP cells[11] were cultured in Dulbecco's modified Eagle medium (DMEM) supplemented with 10% fetal bovine serum (FBS) at 37 °C in 5% CO_2 atmosphere. The cells were passaged every 3−4 days by cell dissociation with trypsin.

Internalization Experiments with Flow Cytometry. HeLa cells were harvested by the incubation with non-enzymatic cell dissociation buffer (CDB-Thermo Scientific) at 37 °C in 5% CO_2 atmosphere for 10−15 min. Cells were centrifuged 2× at 500*g* for 5 min and resuspended in DMEM medium (supplemented with 10% FBS) to a final concentration of 5×10^5 cells per mL. 7.6×10^{-12} M of both biotin-TAT and Cy3 (ratio 1:2) functionalized gold nanoparticles were added to 200 μL of cell suspension and incubated in a 1.5 mL Eppendorf tubes at RT for 2 h on a rotator. Free gold nanoparticles were washed out by centrifugation 2× at 500*g* for 5 min. The cells were resuspended in 500×10^{-6} L PBS and stored on ice until injection into a BD Accuri C6 flow cytometer (BD Biosciences) with a flow rate of 14 μL/min. A gate area was selected from the forward versus side scatter plots and 10,000 events were collected for each sample.

siRNA GFP-Knockdown. *Microfluidic Excitation (Ensemble Treatment).* A 64×10^{-3} m capillary tube with a 20×10^{-6} L capacity was fixed onto a large glass microscope slide with epoxy. Capillary tubing was then assembled onto the ends of the tube and sealed using commercial nail polish. The samples were loaded slowly into upstream tubing of the device using a 50 μL glass syringe (Hamilton). To flow samples through the microcapillary, the samples were pushed with a 1 mL plastic syringe. The cells were collected in an Eppendorf tube. Samples were irradiated with the same laser used in the cell free release studies.

HeLa-GFP cells were harvested with CDB and centrifuged twice at 500*g* for 5 min and resuspended in DMEM medium (supplemented with 10% FBS) to a final concentration of 1×10^6 cells per mL. For each particle type, two concentrations of particles were tested: 7.6×10^{-12} M (2×) and 3.8×10^{-12} M (1×) of siRNA functionalized gold nanoparticles were added to 200 μL of cell suspension and incubated at RT for 2 h on a rotator. Free gold nanoparticles were washed out by centrifugation twice at 500*g* for 5 min. The cells were resuspended in 50×10^{-6} L Hank's Balanced Salt Solution (HBSS) supplemented with 10% FBS and afterward irradiated with 900×10^{-3} W for 30 s through the syringe and tubing system. After irradiation, the cells were transferred to a 6-well plate with DMEM supplemented with 10% FBS and incubated at 37 °C in 5% CO_2 atmosphere. After 72 h the cells are dissociated with trypsin, washed twice at 500*g* for 5 min. The cells were resuspended in 500×10^{-6} L PBS and stored on ice until injection into a BD Accuri C6 flow cytometer with a flow rate of 14×10^{-6} L/min. A gate area selection was determined from the forward versus side scatter plots and 10,000 events were collected for each sample. As a positive control of the GFP-knockdown in HeLa-GFP cells, a reverse transfection StealthTM (Invitrogen) siRNA was carried out. First, 6 pmol siRNA duplex was diluted in 100×10^{-6} L Opti-MEM I Medium without serum in the well of a 24-well tissue well plate and mixed gently. 1×10^{-6} L of Lipofectamine RNAiMAX was added to the diluted siRNA molecules, mixed gently, and incubated for 10−20 min at room temperature. The HeLa-GFP cells were diluted to 50,000 cells in 500×10^{-6} L in DMEM supplemented with 10% FBS and added to the siRNA duplex−Lipofectamine RNAiMAX complexes. This leads to a final volume of 600×10^{-6} L and a final RNA concentration of 10×10^{-9} M. The samples were mixed gently and incubated for 72 h at 37 °C in 5% CO_2. After incubation, the cells were dissociated, washed, and measured at the flow cytometer as described before.

NIR Excitation Confocal Microscopy. Twenty-four hours before the particles were added to the cells, HeLa-GFP cells were split onto Ibidi gridded Petri dishes with 1×10^5 cells for each sample and incubated at 37 °C in 5% CO_2. The next day, cells outside the grid area of the Petri dishes were scraped away and the cells were washed 2× with DPBS. Then, the HeLa-GFP cells were incubated with 7.6×10^{-12} M of siRNA functionalized gold nanoparticles in 200×10^{-6} L DMEM with 10% FBS supplemented at 37 °C in 5% CO_2 atmosphere for 2 h. After washing twice with PBS the cells were stored in 1×10^{-3} L of Hank's buffered saline solution (HBSS) supplemented with 10% FBS for use at the 2-Photon microscope. To activate the siRNA release, the HeLa-GFP cells on gridded Petri dishes were irradiated with a pulsed NIR laser, generated by a two-photon microscope (Olympus Fluoview 1000 MPE). The two-photon microscope was equipped with a 25× water immersion objective (numerical aperture 1.05), a mode-locked titanium-sapphire femtosecond (fs) tunable (690−1020 nm) pulsed laser (100 fs pulse duration, 80 MHz repetition rate, MaiTai HP, Newport-Spectra physics), 473/559/633 nm laser diodes, a transmitted light detection system, and a scan head controlled by Fluoview software. The MaiTai laser was tuned to 800 nm at 8% of the maximum power (~2 mW) and exposed to *z*-stacks (1.4 μM interval) of intended cells through line-by-line scanning (125 kHz) of selected pixels in each *z*-stack (512 × 512 pixels, 0.331 μm per pixel) at 2 μs per pixel. The sample was imaged in a single-photon confocal mode with the blue (for GFP) and green (for Quasar 570 on the siRNA) laser diodes at a scan speed of 80 kHz before and after the exposure to the MaiTai fs laser to compare the fluorescence signal difference caused by the laser treatment. Cells treated with laser and without laser were incubated for 72 h at 37 °C in 5% CO_2 environment and then relocated at the microscope according to the grid information on the bottom of the Petri dish, and imaged in the single-photon confocal mode for GFP or Quasar 570 fluorescence, as well as bright-field images from the transmitted channel.

■ ASSOCIATED CONTENT

Supporting Information

The Supporting Information is available free of charge on the ACS Publications website at DOI: 10.1021/acs.bioconjchem.9b00004.

DOI: 10.1021/acs.bioconjchem.9b00004
Bioconjugate Chem. 2019, 30, 853−860

Optimization of siRNA loading onto each kind of gold nanoparticle; Further characterization of different gold nanoparticles; Spatially controlled knockdown of GFP (PDF)

AUTHOR INFORMATION

Corresponding Author

*E-mail: reich@chem.ucsb.edu.

ORCID

Erin Morgan: 0000-0003-0043-889X

Norbert Reich: 0000-0001-6032-2704

Present Address

[¶]Institute of Pharmacy and Molecular Biotechnology, Ruprecht-Karls University, 69120 Heidelberg, Germany

Author Contributions

[#]E. M. and D. W. gave equal contributions.

Notes

The authors declare no competing financial interest.

ACKNOWLEDGMENTS

This work was supported by the National Institutes of Health (NIH) grant R01 EB012637. The authors thank support of the NRI microscopy center, the Olympus confocal microscope was funded by the NIH grant 1S10RR022585-01A1. The authors thank A. Mikhailovsky for helpful conversations and aid of the UCSB Optical Characterization Facility. The ultrafast laser system used for bulk cell studies was funded by DURIP ARO grant 66886LSRIP.

ABBREVIATIONS

$AgNO_3$, Silver nitrate; CDB, Cell dissociation buffer; CDK, Cyclin dependent factors; CTAB, Hexadecyltrimethylammonium bromide; DEPC, Diethyl dicarbonate; DNA, Deoxyribonucleic acid; GFP, Green fluorescent protein; GNP, Gold nanoparticle; GNR, Gold nanorod; gRNA, Guide RNA; HAuCl4, Hydrogen tetrachloroaurate(III); HCl, Hydrogen chloride; HGNC, Hollow gold nanocage; HGNS, Hollow gold nanoshell; IGF, Insulin growth factors; KCN, Potassium cyanide; $MgCl_2$, Magnesium chloride; miRNA, Micro RNA; mRNA, Messenger RNA; MWCO, Molecular weight cutoff; Na_3Cit, Sodium citrate; Na_3Cit-HCl, Sodium citrate-HCl; $NaBH_4$, Sodium borohydride; NaCl, Sodium chloride; NIR, Near-infrared; OD, Optical density; PBST, 0.1% Tween-20 in Dulbecco's phosphate-buffered saline; RMLP, Rapid modification at low pH; RNA, Ribonucleic acid; RNAi, RNA interference; RNase, Ribonuclease; RT, Room temperature; SDS, Sodium dodecyl sulfate; SH, Sulfhydryl; siRNA, Small interference RNA; SPR, Surface plasmon resonance; TAT, Trans-activator of transcription; TCEP, Tris(2-carboxyethyl)-phosphine HCl; TEM, Transmission electron microscopy; UV−vis, Ultraviolet−visible; VEGF, Vascular endothelial growth factor

REFERENCES

(1) Esteller, M. (2011) Non-Coding RNAs in Human Disease. *Nat. Rev. Genet. 12* (12), 861−874.

(2) Forbes, D. C., and Peppas, N. A. (2012) Oral Delivery of Small RNA and DNA. *J. Controlled Release 162* (2), 438−445.

(3) Hemphill, J., Borchardt, E. K., Brown, K., Asokan, A., and Deiters, A. (2015) Optical Control of CRISPR/Cas9 Gene Editing. *J. Am. Chem. Soc. 137* (17), 5642−5645.

(4) Riboldi, G., Zanetta, C., Ranieri, M., Nizzardo, M., Simone, C., Magri, F., Bresolin, N., Comi, G. P., and Corti, S. (2014) Antisense Oligonucleotide Therapy for the Treatment of C9ORF72 ALS/FTD Diseases. *Mol. Neurobiol. 50* (3), 721−732.

(5) Draz, M. S., Fang, B. A., Zhang, P., Hu, Z., Gu, S., Weng, K. C., Gray, J. W., and Chen, F. F. (2014) Nanoparticle-Mediated Systemic Delivery of SiRNA for Treatment of Cancers and Viral Infections. *Theranostics 4* (9), 872−892.

(6) Fire, A., Xu, S., Montgomery, M. K., Kostas, S. A., Driver, S. E., and Mello, C. C. (1998) Potent and Specific Genetic Interference by Double-Stranded RNA in Caenorhabditis Elegans. *Nature 391* (6669), 806−811.

(7) Bumcrot, D., Manoharan, M., Koteliansky, V., and Sah, D. W. Y. (2006) RNAi Therapeutics: A Potential New Class of Pharmaceutical Drugs. *Nat. Chem. Biol. 2* (12), 711−719.

(8) Li, J., Xue, S., and Mao, Z.-W. (2016) Nanoparticle Delivery Systems for SiRNA-Based Therapeutics. *J. Mater. Chem. B 4* (41), 6620−6639.

(9) Whitehead, K. A., Langer, R., and Anderson, D. G. (2009) Knocking down Barriers: Advances in SiRNA Delivery. *Nat. Rev. Drug Discovery 8* (2), 129−138.

(10) Huang, X., Lai, Y., Braun, G. B., and Reich, N. O. (2017) Modularized Gold Nanocarriers for TAT-Mediated Delivery of SiRNA. *Small 13* (8), 1602473.

(11) Huang, X., Hu, Q., Lai, Y., Morales, D. P., Clegg, D. O., and Reich, N. O. (2016) Light-Patterned RNA Interference of 3D-Cultured Human Embryonic Stem Cells. *Adv. Mater. 28* (48), 10732−10737.

(12) Morales, D. P., Braun, G. B., Pallaoro, A., Chen, R., Huang, X., Zasadzinski, J. A., and Reich, N. O. (2015) Targeted Intracellular Delivery of Proteins with Spatial and Temporal Control. *Mol. Pharmaceutics 12* (2), 600−609.

(13) Morales, D. P., Wonderly, W. R., Huang, X., McAdams, M., Chron, A. B., and Reich, N. O. (2017) Affinity-Based Assembly of Peptides on Plasmonic Nanoparticles Delivered Intracellularly with Light Activated Control. *Bioconjugate Chem. 28* (7), 1816−1820.

(14) Morales, D. P., Morgan, E. N., McAdams, M., Chron, A. B., Shin, J. E., Zasadzinski, J. A., and Reich, N. O. (2018) Light-Triggered Genome Editing: Cre Recombinase Mediated Gene Editing with Near-Infrared Light. *Small 14* (30), 1800543.

(15) Link, S., and El-Sayed, M. A. (1999) Spectral Properties and Relaxation Dynamics of Surface Plasmon Electronic Oscillations in Gold and Silver Nanodots and Nanorods. *J. Phys. Chem. B 103* (40), 8410−8426.

(16) Link, S., and El-Sayed, M. A. (2000) Shape and Size Dependence of Radiative, Non-Radiative and Photothermal Properties of Gold Nanocrystals. *Int. Rev. Phys. Chem. 19*, 409−453.

(17) Daniel, M.-C., and Astruc, D. (2004) Gold Nanoparticles: Assembly, Supramolecular Chemistry, Quantum-Size-Related Properties, and Applications toward Biology, Catalysis, and Nanotechnology. *Chem. Rev. 104* (1), 293−346.

(18) Dreaden, E. C., Alkilany, A. M., Huang, X., Murphy, C. J., and El-Sayed, M. A. (2012) The Golden Age: Gold Nanoparticles for Biomedicine. *Chem. Soc. Rev. 41* (7), 2740−2779.

(19) Huang, X., Pallaoro, A., Braun, G. B., Morales, D. P., Ogunyankin, M. O., Zasadzinski, J., and Reich, N. O. (2014) Modular Plasmonic Nanocarriers for Efficient and Targeted Delivery of Cancer-Therapeutic SiRNA. *Nano Lett. 14* (4), 2046−2051.

(20) Jain, P. K., Qian, W., and El-Sayed, M. A. (2006) Ultrafast Cooling of Photoexcited Electrons in Gold Nanoparticle−Thiolated DNA Conjugates Involves the Dissociation of the Gold−Thiol Bond. *J. Am. Chem. Soc. 128* (7), 2426−2433.

(21) Lukianova-Hleb, E. Y., Belyanin, A., Kashinath, S., Wu, X., and Lapotko, D. O. (2012) Plasmonic Nanobubble-Enhanced Endosomal Escape Processes for Selective and Guided Intracellular Delivery of Chemotherapy to Drug-Resistant Cancer Cells. *Biomaterials 33* (6), 1821−1826.

(22) Huschka, R., Zuloaga, J., Knight, M. W., Brown, L. V., Nordlander, P., and Halas, N. J. (2011) Light-Induced Release of

DOI: 10.1021/acs.bioconjchem.9b00004
Bioconjugate Chem. 2019, 30, 853−860

DNA from Gold Nanoparticles: Nanoshells and Nanorods. *J. Am. Chem. Soc. 133* (31), 12247−12255.
(23) Christie, C., Madsen, S. J., Peng, Q., and Hirschberg, H. (2017) Photothermal Therapy Employing Gold Nanoparticle- Loaded Macrophages as Delivery Vehicles: Comparing the Efficiency of Nanoshells Versus Nanorods. *J. Environ. Pathol., Toxicol. Oncol. 36* (3), 229−235.
(24) Yue, J., Feliciano, T. J., Li, W., Lee, A., and Odom, T. W. (2017) Gold Nanoparticle Size and Shape Effects on Cellular Uptake and Intracellular Distribution of SiRNA Nanoconstructs. *Bioconjugate Chem. 28* (6), 1791−1800.
(25) Jiang, X., Qu, W., Pan, D., Ren, Y., Williford, J.-M., Cui, H., Luijten, E., and Mao, H.-Q. (2013) Plasmid-Templated Shape Control of Condensed DNA-Block Copolymer Nanoparticles. *Adv. Mater. 25* (2), 227−232.
(26) Williford, J.-M., Ren, Y., Huang, K., Pan, D., and Mao, H.-Q. (2014) Shape Transformation Following Reduction-Sensitive PEG Cleavage of Polymer/DNA Nanoparticles. *J. Mater. Chem. B 2* (46), 8106−8109.
(27) Sun, Y., and Xia, Y. (2004) Mechanistic Study on the Replacement Reaction between Silver Nanostructures and Chloroauric Acid in Aqueous Medium. *J. Am. Chem. Soc. 126* (12), 3892−3901.
(28) Hong, Y., Huh, Y.-M., Yoon, D. S., and Yang, J. (2012) Nanobiosensors Based on Localized Surface Plasmon Resonance for Biomarker Detection. *J. Nanomater. 2012*, 1−13.
(29) Zhang, X., Chen, Y. L., Liu, R.-S., and Tsai, D. P. (2013) Plasmonic Photocatalysis. *Rep. Prog. Phys. 76* (4), 046401.
(30) Zhang, X., Servos, M. R., and Liu, J. (2012) Instantaneous and Quantitative Functionalization of Gold Nanoparticles with Thiolated DNA Using a PH-Assisted and Surfactant-Free Route. *J. Am. Chem. Soc. 134* (17), 7266−7269.
(31) Braun, G. B., Pallaoro, A., Wu, G., Missirlis, D., Zasadzinski, J. A., Tirrell, M., and Reich, N. O. (2009) Laser-Activated Gene Silencing *via* Gold Nanoshell−siRNA Conjugates. *ACS Nano 3* (7), 2007−2015.
(32) Whitney, M., Savariar, E. N., Friedman, B., Levin, R. A., Crisp, J. L., Glasgow, H. L., Lefkowitz, R., Adams, S. R., Steinbach, P., Nashi, N., et al. (2013) Ratiometric Activatable Cell-Penetrating Peptides Provide Rapid In Vivo Readout of Thrombin Activation. *Angew. Chem., Int. Ed. 52* (1), 325−330.
(33) Xue, C., Xue, Y., Dai, L., Urbas, A., and Li, Q. (2013) Size- and Shape-Dependent Fluorescence Quenching of Gold Nanoparticles on Perylene Dye. *Adv. Opt. Mater. 1* (8), 581−587.
(34) Prevo, B., Esakoff, S., Mikhailovsky, A., and Zasadzinski, J. (2008) Scalable Routes to Gold Nanoshells with Tunable Sizes and Response to Near-Infrared Pulsed Laser Irradiation. *Small 4*, 1183−1195.
(35) Skrabalak, S. E., Chen, J., Au, L., Lu, X., Li, X., and Xia, Y. (2007) Gold Nanocages for Biomedical Applications. *Adv. Mater. 19*, 3177−3184.
(36) Shi, D., Song, C., Jiang, Q., Wang, Z.-G., and Ding, B. (2013) A Facile and Efficient Method to Modify Gold Nanorods with Thiolated DNA at a Low PH Value. *Chem. Commun. 49*, 2533.

DOI: 10.1021/acs.bioconjchem.9b00004
Bioconjugate Chem. 2019, 30, 853−860